

PAPER • OPEN ACCESS

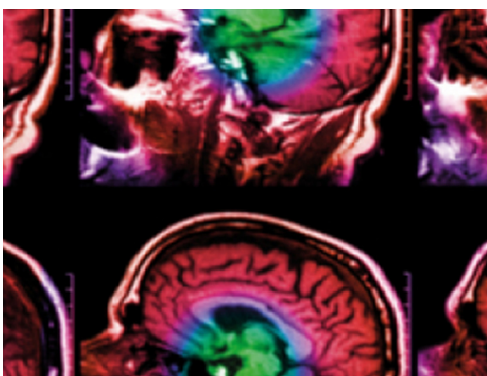
Modelling the effects of quinidine, disopyramide, and E-4031 on short QT syndrome variant 3 in the human ventricles

To cite this article: Cunjin Luo *et al* 2017 *Physiol. Meas.* **38** 1859

View the [article online](#) for updates and enhancements.

Related content

- [Simulation of Brugada syndrome using cellular and three-dimensional whole-heart modeling approaches](#)
Ling Xia, Yu Zhang, Henggui Zhang *et al.*
- [Transition from ventricular fibrillation to ventricular tachycardia: a simulation study on the role of \$Ca^{2+}\$ -channel blockers in human ventricular tissue](#)
O Bernus, B Van Eyck, H Verschelde *et al.*
- [Cell model for efficient simulation of wave propagation in human ventricular tissue under normal and pathological conditions](#)
K H W J Ten Tusscher and A V Panfilov



IPEM | IOP

Series in Physics and Engineering in Medicine and Biology

Your publishing choice in medical physics,
biomedical engineering and related subjects.

Start exploring the collection—download the
first chapter of every title for free.

Modelling the effects of quinidine, disopyramide, and E-4031 on short QT syndrome variant 3 in the human ventricles

Cunjin Luo¹ , Kuanquan Wang¹ and Henggui Zhang^{1,2,3}

¹ School of Computer Science and Technology, Harbin Institute of Technology (HIT), Harbin 150001, People's Republic of China

² School of Physics and Astronomy, The University of Manchester, Manchester M13 9PL, United Kingdom

³ Space Institute of Southern China, Shenzhen 518117, People's Republic of China

E-mail: wangkq@hit.edu.cn (K Wang) and H.Zhang-3@manchester.ac.uk (H Zhang)

Received 22 April 2017, revised 13 August 2017

Accepted for publication 16 August 2017

Published 21 September 2017



CrossMark

Abstract


Objective: Short QT syndrome (SQT3) is an inherited cardiac channelopathy, but at present little information is available on its pharmacological treatment. SQT3 variant (linked to the inward rectifier potassium current I_{K1}) of SQT3, results from a gain-of-function mutation (Kir2.1 D172N) in the *KCNJ2*-encoded channels, which is associated with ventricular fibrillation (VF). Using biophysically-detailed human ventricular computer models, this study investigated the potential effects of quinidine, disopyramide, and E-4031 on SQT3. **Approach:** The ten Tusscher *et al* model of human ventricular myocyte action potential (AP) was modified to recapitulate the changes in I_{K1} due to heterozygous and homozygous forms of the D172N mutation. Wild-type (WT) and mutant WT-D172N and D172N formulations were incorporated into one-dimensional (1D) and 2D tissue models with transmural heterogeneities. Effects of drugs on channel-blocking activity were modelled using half-maximal inhibitory concentration (IC_{50}) and Hill coefficient (nH) values. Effects of drugs on AP duration (APD), effective refractory period (ERP) and QT interval of pseudo-ECGs were quantified, and both temporal and spatial vulnerability to re-entry was measured. Re-entry was simulated in the 2D ventricular tissue. **Main results:** At the single cell level, the drugs quinidine, disopyramide, and E-4031 prolonged APD at 90% repolarization (APD_{90}), and decreased maximal transmural voltage heterogeneity (δV); this



Original content from this work may be used under the terms of the [Creative Commons Attribution 3.0 licence](https://creativecommons.org/licenses/by/3.0/). Any further distribution of this work must maintain attribution to the author(s) and the title of the work, journal citation and DOI.

caused the decreased transmural dispersion of APD₉₀. Quinidine prolonged the QT interval and decreased the T-wave amplitude. Furthermore, quinidine increased ERP and reduced temporal vulnerability and increased spatial vulnerability, resulting in a reduced susceptibility to arrhythmogenesis in SQT3. In the 2D tissue, quinidine was effective in terminating and preventing re-entry associated with the heterozygous D172N condition. Quinidine exhibited significantly better therapeutic effects on SQT3 than disopyramide and E-4031. *Significance:* This study substantiates a causal link between quinidine and QT interval prolongation in SQT3 Kir2.1 mutations and highlights possible pharmacological agent quinidine for treating SQT3 patients.

Keywords: short QT syndrome, computational modelling, arrhythmia, quinidine, disopyramide, E-4031

 Supplementary material for this article is available [online](#)

(Some figures may appear in colour only in the online journal)

Introduction

Short QT syndrome (SQTs) is a disorder in the electrical function of the heart, and it is associated with high risk of arrhythmias and of sudden cardiac death (SCD) (Gussak *et al* 2000, Gaita *et al* 2003, Schimpf *et al* 2005). The SQTs phenotype is characterized by less than 360 ms with a range of 220–360 ms and a higher, symmetrical T-wave amplitude on the electrocardiogram (ECG). The ‘short QT interval’ was first discovered as a new clinical entity by Gussak *et al* (2000) in 2000 and first described with arrhythmias and a high incidence of SCD in families with SQTs by Gaita *et al* (2003) in 2003. The basis for SQTs associated with various mutations in 6 different genes have been found: *KCNH2* (Brugada *et al* 2004), *KCNQ1* (Bellocq *et al* 2004), *KCNJ2* (Priori *et al* 2005), *CACNA1C* (Antzelevitch *et al* 2007), *CACNB2b* (Antzelevitch *et al* 2007), and *CACNA2D1* (Templin *et al* 2011). Among these mutations, either a gain-in-function of the potassium channel (linked to *KCNH2*, *KCNQ1*, and *KCNJ2* gene) or a loss-in-function of the calcium channel (linked to *CACNA1C*, *CACNB2b*, and *CACNA2D1* gene) has been observed.

Among the mutations is a pair of complementary nucleotide bases substitute from aspartic acid (also known as aspartate) to sparagine at position 172 in *KCNJ2* (which encodes the Kir2.1 channel protein) in patients exhibiting a history of palpitations, presyncope, and syncope symptoms (Priori *et al* 2005). Analysis of wild-type (WT) Kir2.1, of Kir2.1 D172N mutation under heterozygous (WT-D172N) homozygous (D172N) conditions, revealed the mutation led to changes in the inward rectifier potassium current (I_{K1}) channels, which results in a gain-in-function, producing an increase of I_{K1} (Priori *et al* 2005). Previous studies have been shown that increased I_{K1} in SQT3 shortened the action potential duration (APD) and the effective refractory period (ERP), and stabilized rotors in computational models of human ventricular electrophysiology (Adeniran *et al* 2012).

The current first-line treatment for SQTs patients is an implantable cardioverter-defibrillator (ICD) device, but there is an increased risk of inappropriate treatment due to tachycardia, atrial fibrillation and, above all, of T-wave oversensing (Schimpf *et al* 2003). Moreover, the QT interval does not fall within the normal range over time by using the ICD. Clinical trials from Gaita *et al* (2004) concurrent with the *in vitro* findings demonstrated the antiarrhythmic

effectiveness of quinidine in patients with SQTs. They reported hydroquinidine administration prolonged the QT interval to the normal range. Moreover, quinidine also restored the QT interval/heart rate (QT-RR) relationship towards the normal range (Wolpert *et al* 2005). In a one-year follow-up, the SQT1 patients who treat hydroquinidine remained asymptomatic, and no further episode of arrhythmias was detected. However, the mechanisms by which quinidine prolongs QT interval and terminates and prevents arrhythmias in SQTs have still not yet been fully elucidated. However, possibly due to a lack of phenotypically accurate experimental models, there has hitherto not been any detailed investigation of how the quinidine prolongs QT interval and terminates and prevents ventricular arrhythmias in SQTs. Therefore, this study aimed to evaluate and compare the potential effects of quinidine in comparison to disopyramide and E-4031 on ventricular depolarization and repolarization and susceptibility to re-entrant excitation waves in SQT3, by using multi-scale models of human ventricular electrophysiology. These results may provide theoretical insights into the possible pharmacological agent for treating SQT3 patients.

Methods

I_{K1} and human ventricular cell models

A contemporary human ventricular cell action potential (AP) model developed by ten Tusscher and Panfilov (2006) was used for the simulations in this study. The original equations for *I_{K1}* in the ten Tusscher *et al* model was modified to incorporate the previously reported changes in *I_{K1}* for WT, mutant D172N and WT-D172N conditions (Priori *et al* 2005). The derived equation of *I_{K1}* for WT, WT-D172N and D172N conditions (McPate *et al* 2008) is available in the supplementary materials (stacks.iop.org/PM/38/1859/mmedia).

In a single myocyte, the electrophysiological behavior can be described using the following ordinary differential equation (ODE):

$$\frac{dV}{dt} = -\frac{I_{\text{ion}} + I_{\text{stim}}}{C_m} \quad (1)$$

where *V* is the cell membrane potential; *t* is time; *C_m* is the membrane capacitance per unit area; *I_{stim}* is the external stimulus current; *I_{ion}* is the sum of membrane currents. Particularly, the component of the late sodium current (*I_{NaL}*) from the ORd model (O'Hara *et al* 2011) was incorporated. Equation (1) was numerically integrated using the forward Euler method with a time step of 0.02 ms. APs were elicited with an S1-S2 protocol consisting of 20 S1 stimuli and an S2 stimulus. The S1 was applied at a basic cycle length (BCL) of 800 ms and -52 pA/pF strength for 1 ms. The S2 was applied at varying diastolic intervals (DI) after the AP evoked by the last S1. The ERP was measured as the smallest DI for which the overshoot of the AP evoked by the S2 reached 80% of the AP evoked by the 20th S1.

Modelling the interactions between drugs and ion channels

A 'simple pore block' theory (Brennan *et al* 2009) was implemented to model drug-ion channel binding interactions. The reduced maximum conductances of the targeted channels in the presence of quinidine, disopyramide, and E-4031 were shown in tables 1–3, respectively. E-4031 is a specific blocker of delayed rectifier current (*I_{Kr}*) (Izumi *et al* 2010), and it does not affect sodium and calcium inward currents (Wettwer *et al* 1991). However, quinidine and disopyramide are multi-channel blockers (Sanchez-Chapula 1999, Gaita *et al* 2004). In this

Table 1. Conductivities (% of the original value) in the presence of 4100, and 1000 nM E-4031.

Current	IC ₅₀	nH	Conductivity	Source
<i>I</i> _{Kr}	15.96 ± 0.04 nM	0.74 ± 0.05	80.0/22.1/2.9%	McPate <i>et al</i> (2006, 2008)

Table 2. Conductivities (% of the original value) in the presence of 13 and 100 μM disopyramide.

Current	IC ₅₀	nH	Conductivity	Source
<i>I</i> _{Kr}	10.66 ± 0.04 μM	1.07 ± 0.05	39.1/5.4%	McPate <i>et al</i> (2006, 2008)
<i>I</i> _{Na}	168.4 μM	1.09	95/63.6%	Yasuda <i>et al</i> (2015)
<i>I</i> _{to}	259 μM	1.07	94.3/75.5%	Sanchez-Chapula (1999)
<i>I</i> _{CaL}	1036.7 μM	1.0	98.7/90.9%	Yasuda <i>et al</i> (2015)

Table 3. Conductivities (% of the original value) in the presence of 4, 7, and 10 μM quinidine.

Current	IC ₅₀	nH	Conductivity	Source
<i>I</i> _{Kr}	0.62 ± 0.03 μM	0.93 ± 0.06	17.0/10.0/7.0%	McPate <i>et al</i> (2006, 2008)
<i>I</i> _{Ks}	4.899 μM	1.4	56.9/37.5/27.0%	Crumb <i>et al</i> (2016)
<i>I</i> _{to}	3.487 μM	1.3	45.6/28.8/20.3%	Crumb <i>et al</i> (2016)
<i>I</i> _{Na}	14.6 μM	1.22	83.0/71.1/61.4%	Kramer <i>et al</i> (2013)
<i>I</i> _{CaL}	14.9 ± 1.5 μM	1.1 ± 0.1	83.2/72.9/61.29%	Zhang and Hancox (2002)
<i>I</i> _{NaCa}	Not given	Not given	95.0/90.0/86.52%	Zhang and Hancox (2002)
<i>I</i> _{NaL}	12.0 ± 0.7 μM	1.0	71.7/62.3/47.7%	Wu <i>et al</i> (2008)

study, several doses (4, 7, and, 10 03BCM for quinidine; 13 and 100 μM for disopyramide; 4, 100, and 1000 nM for E-4031) were selected to assess the pharmacological effects on SQT3.

Effects of a combined action of blocking of multiple currents in the presence of quinidine at 4, 7, and 10 μM doses together with different theoretical (5% and 10%) and experimental (13.5%) blocking of *I*_{NaCa}.

Multicellular tissue simulations

Propagation of APs in multicellular tissue was described by using the monodomain equation:

$$\frac{\partial V}{\partial t} = -\frac{I_{ion} + I_{stim}}{C_m} + \nabla \cdot (D\nabla V) \tag{2}$$

where ∇ is the gradient operator; *D* is the diffusion parameter modelling the intercellular electrical coupling via gap junctions. *D* was set to a value of 0.0008 cm² ms⁻¹ that gave a conduction velocity (CV) of a planar wave at 52 cm/s, close to the experimental CV of ~50 cm s⁻¹ through one-dimensional (1D) strand (Weingart 1977, Taggart *et al* 2000), except for a 5-fold decrease at the MIDDLE-EPI junction (Gima and Rudy 2002). The strand had a total length of 15 mm, with space step 0.15 mm, which is close to the cell length of a human ventricular myocyte (80–150 μm). The corresponding length of each subregion was 3.75 mm for 25 ENDO cells, 5.25 mm for 35 MIDDLE cells, and 6 mm for 40 EPI cells of the strand. The total length and proportion of each sub-region reliably reproduced a positive T wave (Zhang

et al 2008, Adeniran *et al* 2011, 2012). The pseudo-ECG was computed by using the Gima and Rudy approach (Gima and Rudy 2002). The electrode was placed at a site located 2.0 cm from the ENDO distal end. The pseudo-ECG morphology is consistent with the clinical data (Priori *et al* 2005).

A two-dimensional (2D) model was modelled by expanding the 1D strand (length of 15 mm- x direction, 100 cells) into a sheet with a width (y direction, 1000 cells) of 150 mm (or with a larger size in order to measure the critical size of the tissue to support the formation and maintenance of re-entry). The spatial and time steps were the same as used in the 1D strand. Re-entry was initiated in 2D tissue by an S1–S2 protocol. An S1 (amplitude: -52 pA/pF; duration: 1 ms) was applied at ENDO distal end of the 2D tissue (length: 15 mm along the x - direction; width: 150 mm in the y - direction) to evoke a planar wave. During the vulnerable window (VW), an S2 with the same amplitude and duration as S1 was applied to the MIDDLE-EPI junction to evoke a unidirectional wave propagation. The S2 has variable spatial sizes. The critical size of the tissue to support re-entry was quantified as the minimum length of S2 that supports the formulation and maintenance of re-entry, which provides a reciprocal index of the spatial vulnerability of ventricle to re-entry: the smaller the critical size, the easier the initiation of re-entry (Zhang *et al* 2008).

Results

Effects of quinidine, disopyramide, and E-4031 on SQT3 in the single cell APs

The ten Tusscher *et al* human ventricular cell model (ten Tusscher and Panfilov 2006) incorporating SQT3 I_{K1} formulations (Adeniran *et al* 2012) gave AP characteristics which were in excellent agreement with experimental data from human ventricular myocytes (Priori *et al* 2005). Alternations to I_{K1} due to SQT3 mutations accelerated the repolarization phase of APs as shown in figure 1. The D172N mutation resulted in shortening of APD, with the D172N condition exerting a more profound effect than the WT-D172N condition. The measured APD₉₀ was 302 ms for the ENDO (figure 1(a)), 406 ms for the MIDDLE (figure 1(d)), and 304 ms for the EPI (figure 1(g)) in WT, which was shortened, respectively, to 273, 357, and 274 ms in WT-D172N and to 261, 341, and 262 ms in D172N condition. The abbreviated APD resulted largely from increased I_{K1} during the late phase of AP repolarization as shown by the time course of I_{K1} and the I - V phase plot in figures 1(b), (c), (e), (f), (h) and (i).

The effects of drug interactions simulated on APD prolongation from representative ENDO myocytes under WT-D172N and D172N condition are summarized in figure 2. APD₉₀ in WT-D12N condition was prolonged to 278, 293, 299, 288, 291, 321, 340, and 341 ms in the presence of 4, 100, and 1000 nM E-4031, 13 and 100 μ M disopyramide, and 4, 7, and 10 μ M quinidine, respectively, and in D172N condition was prolonged to 266, 279, 284, 274, 276, 303, 319, and 320 ms, respectively. Quinidine produced a significant prolongation of APD₉₀, bringing it much closer to that in WT condition. The observed resting membrane potential (RP) values were -84.65 , -85.61 , -85.42 , -86.06 , and -85.97 mV for the WT, WT-D172N, WT-D172N + 4 μ M quinidine, D172N, and D172N + 4 μ M quinidine conditions, respectively.

Effects of quinidine, disopyramide, and E-4031 on SQT3 in the 1D strand model

The simulated effects of all drug interactions simulated on pseudo-ECG are shown in figure 3. Supra-threshold stimulus (-52 pA/pF) was applied to the ENDO distal end, initiating electrical excitation propagation towards MIDDLE and EPI parts in figure 3(a) (for WT-D172N

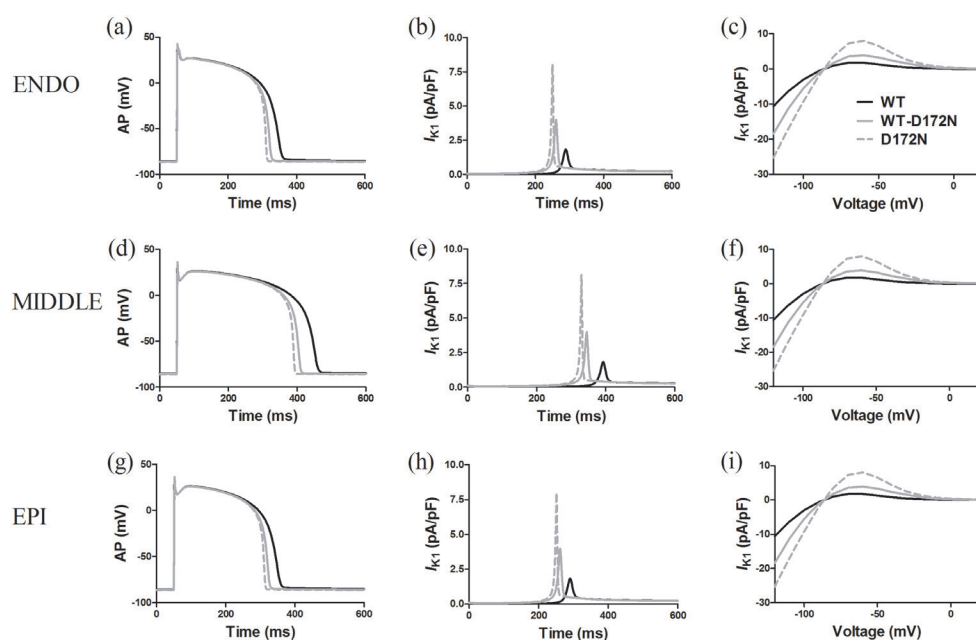


Figure 1. Simulated AP profiles, I_{K1} traces and $I-V$ relationships in WT, mutant WT-D172N and D172N conditions. AP profiles for ENDO (a), MIDDLE (d), and EPI (g) cells. Corresponding I_{K1} traces for ENDO (b), MIDDLE (e), and EPI (h) cells. Instantaneous $I-V$ relations for ENDO (c), MIDDLE (f), and EPI (i) cells.

condition), (b) (for WT-D172N + 4 μM quinidine condition), (e) (for D172N condition), and (f) (for D172N + 4 μM quinidine condition). From this electrical excitation wave, pseudo-ECG traces were computed as shown in figures 3(c) and (g). In these simulation results, quinidine, disopyramide, and E-4031 prolonged the QT intervals on the ECGs and reduced the T-wave amplitude. The QT interval was prolonged from 322 ms in WT-D172N condition to 328, 346, 353, 340, 347, 380, 395, and 397 ms in the presence of 4, 100, and 1000 nM E-4031, 13, and 100 μM , and 4, 7, and 10 μM quinidine, respectively, and from 318 ms in the D172N condition to 323, 328, 333, 338, 364, 371, 375 ms, respectively. Then we further measured the rate dependence of ventricular CV (shown in supplementary materials). It shows that quinidine decreased ventricular conduction. At a rate of 75 b.p.m. (Pacing Cycle Length (PCL) = 800 ms), the measured CV was 52 cm s^{-1} for the WT, 51 cm/s for the WT-D172N, 47 cm/s for the D172N, 41 cm s^{-1} for the WT-D172N + 10 μM quinidine, and 36 cm/s for the D172N + 10 μM quinidine conditions. The decreased CV was due to the blocked sodium current as shown in table 2, as no change in the intercellular coupling was considered.

In order to explain the decreased T-wave amplitude seen in figure 3(c), we examined the effects of quinidine on the membrane potential heterogeneity (δV) during APs, as well as transmural APD dispersion across the strand. Figures 4(a) and (b) show simulated ENDO, MIDDLE, and EPI APs with WT-D172N, and WT-D172N + 4 μM quinidine conditions whilst figures 4(c) and (d) show corresponding time-course plots of the δV between different cell types. The δV maximal between both MIDDLE-EPI and ENDO-MIDDLE APs was smaller with actions of drugs than before (see figures 4(e) and (f)). Figure 5(a) shows the distribution of APD_{90} for WT, WT-D172M and WT-D172N + 4 μM quinidine conditions.

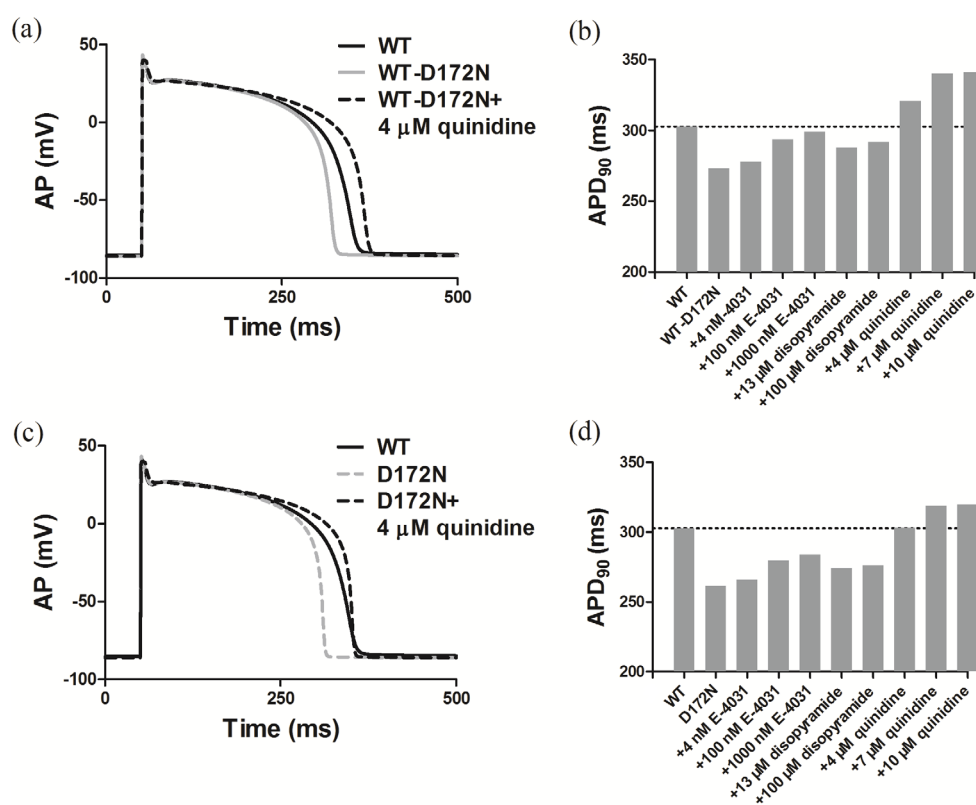


Figure 2. Simulated effects of quinidine, disopyramide, and E-4031 on SQT3 in single ENDO cell APs. AP profiles for mutant WT-D172N (a) and D172N (c) conditions by using the modified model. Measured APD₉₀ for mutant WT-D172N (b) and D172N (d) conditions.

Quinidine decreased APD₉₀ dispersion of APD₉₀ in the 1D strand in figure 5(b). Figures 5(c) and (d) show the maximal spatial gradient of APD₉₀ in drug-in-action conditions.

The ERP was prolonged in all drug-in-action conditions compared to the mutant conditions (see figure 6). ERP restitution (ERP-R) in the presence of quinidine showed a rightward shift, with decreased maximal slopes, which is associated with decreased instability of re-entrant excitation waves (Xie *et al* 2002), indicating antiarrhythmic effects of quinidine on D172N mutation. Then we quantified the vulnerability of tissue to unidirectional conduction block. Results of bidirectional conduction block, unidirectional conduction block, and bi-directional conduction are shown in figures 6(e)–(g), respectively. Figures 6(h) and (i) demonstrate the width of the VW. The VW decreased from 15 ms in WT-D172N to 7 ms in WT-D172N + 4 μM quinidine condition, and from 36 ms in D172N to 11 ms in D172N + 4 μM quinidine condition.

Effects of quinidine, disopyramide, and E-4031 on SQT3 in 2D model

Further simulations were performed utilizing an idealized area of the 2D model to investigate the effects of quinidine, disopyramide, and E-4031 on the dynamic behaviours of re-entrant excitation waves. The results are shown in figure 7, in which snapshots of re-entrant excitation

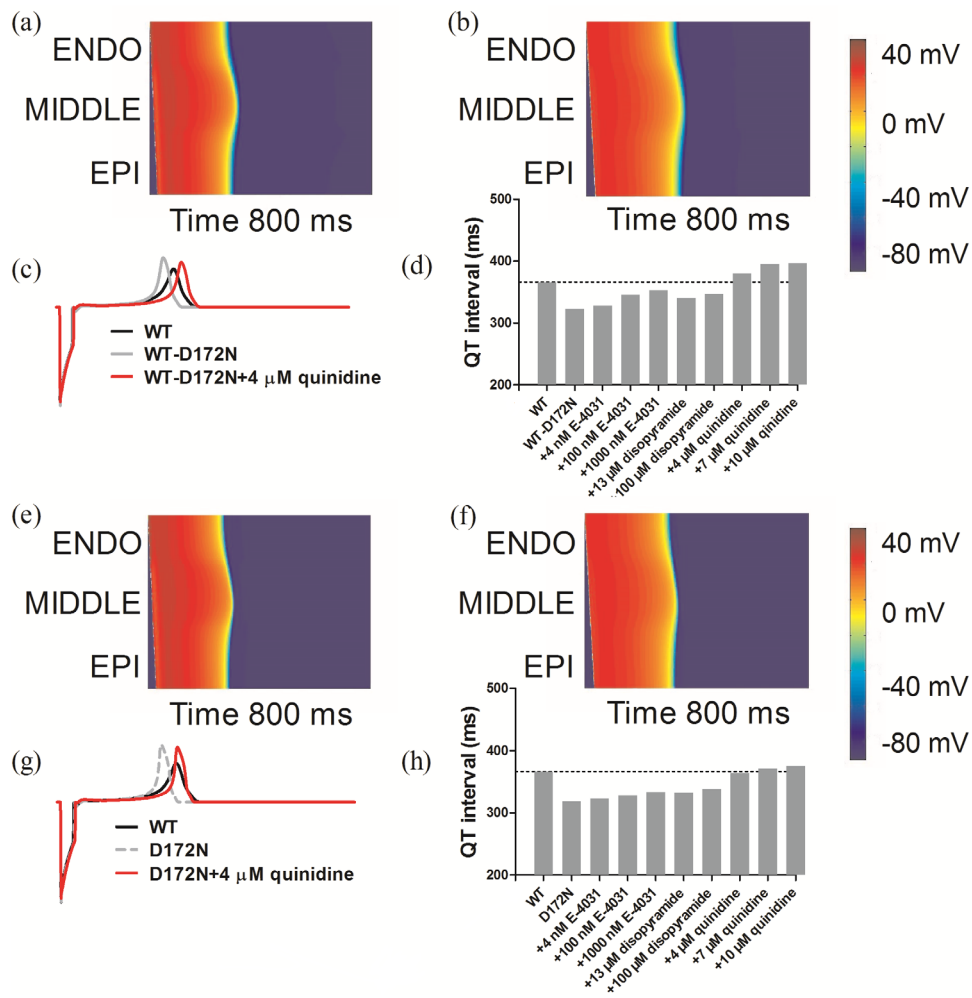


Figure 3. Space-time plot of AP prolongation across a 1D strand and the simulated pseudo-ECG and QT intervals. (a) Space-time plot of AP prolongation in WT-D172N condition. (b) Space-time plot of AP prolongation in WT-D172N + 4 μ M quinidine condition. (c) Superimposed pseudo-ECGs in WT-D172N + drugs conditions. (d) Corresponding QT intervals in WT-D172N + drugs conditions. (e) Space-time plot of AP prolongation in D172N condition. (f) Space-time plot of AP prolongation in D172N + 4 μ M quinidine condition. (g) Superimposed pseudo-ECGs in D172N + drugs conditions. (h) Corresponding QT intervals in D172N + drugs conditions.

waves from WT, WT-D172N, and WT-D172N + 4 μ M quinidine conditions are shown. In WT condition (see figures 6(a)–(d)), re-entrant waves were unstable and non-stationary as the tip of the re-entry meandered out of the tissue boundaries leading to self-termination, whereas augmented I_{K1} in the WT-D172N condition (see figures 6(f)–(i)) helped to sustain re-entrant excitation waves. Snapshots of simulated pharmacological effects of quinidine on re-entry in WT-D172N condition are shown in figures 6(k)–(n). Quinidine terminated re-entrant excitation waves in the WT-D172N condition. Figures 6(e), (j) and (o) show a recording of the evolution of the AP of an EPI cell in the tissue in WT, WT-D172N, and WT-D172N + 4 μ M quinidine conditions, respectively.

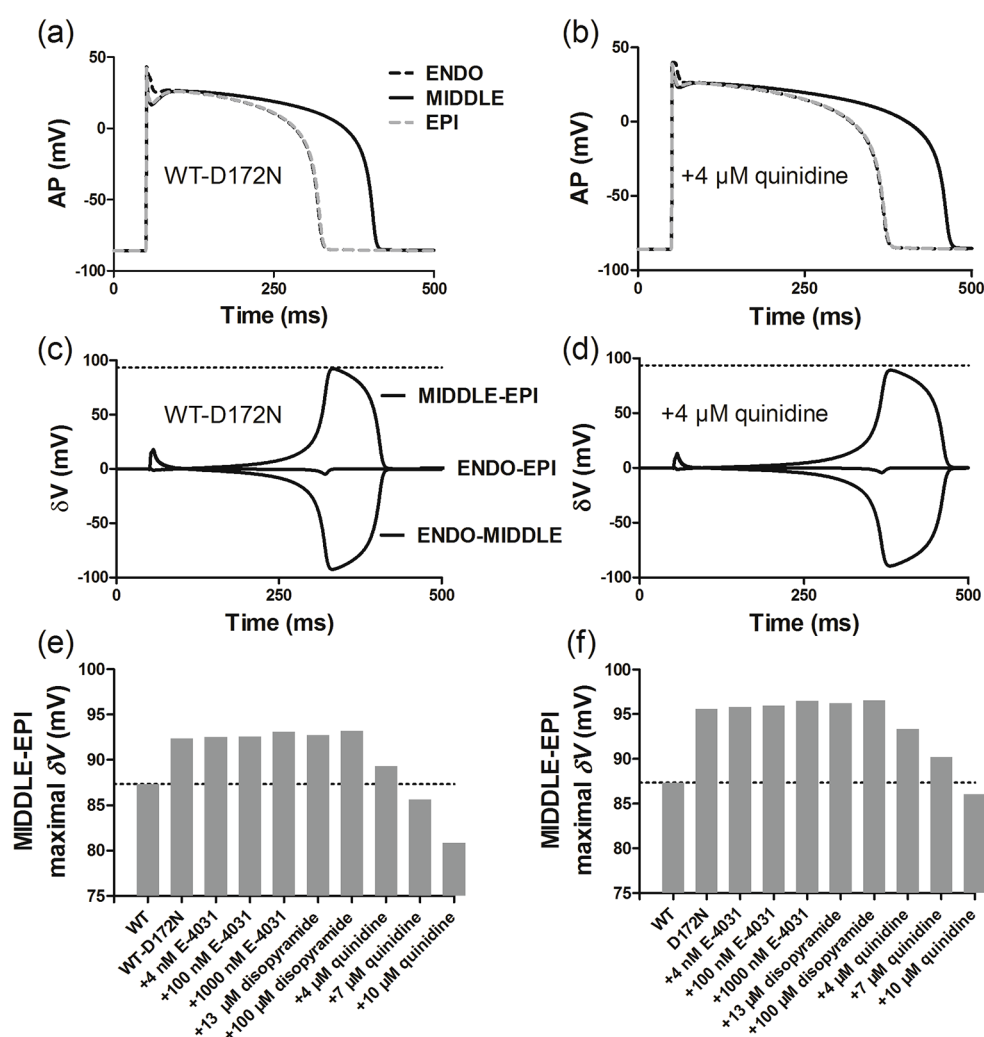


Figure 4. Membrane potential heterogeneity (δV) between ENDO, MIDDLE, and EPI cells. (a) and (b) ENDO, MIDDLE, and EPI APs in WT-D172N and WT-D172N + 4 μM quinidine conditions, respectively. (c) and (d) Corresponding plots of δV against time. (e) and (f) Maximal δV during repolarization process between MIDDLE-EPI cells.

We then proceeded to measure the minimal spatial length of a premature S2 stimulus that provides a sufficient substrate for the formulation and maintenance of re-entry. Quinidine, disopyramide, and E-4031 prolonged the minimal length of S2; the minimal length was prolonged from 78 mm in WT-D12N condition to 79, 81, 82, 85, 87, 107, 110, and 112 mm in the presence of 4, 100, and 1000 nM E-4031, 13 and 100 μM disopyramide, and 4, 7, and 10 μM quinidine, respectively, and prolonged from 68 mm in D172N condition to 70, 73, 74, 76, 78, 90, 95, and 97 mm, respectively. Prolongation of APD due to the action of drugs increased the wavelength of the wave and thus increased the minimal length of S2, which supports the notion that in SQT3 tissue with the application of quinidine, re-entrant excitation waves occur harder than in the drug-free SQT3 tissue.

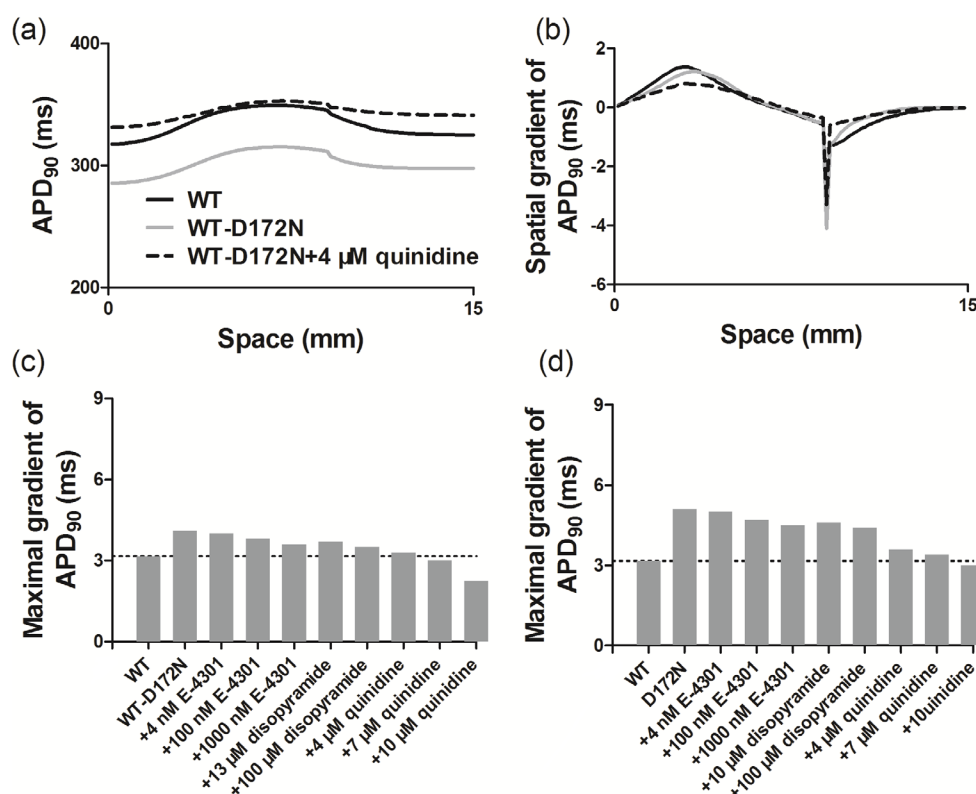


Figure 5. APD₉₀ distribution and its spatial gradient in a 1D strand. (a) Spatial distribution of APD₉₀ in WT, WT-D172N, and WT-D172N + 4 μM quinidine conditions. (b) The spatial gradient of APD₉₀ in WT, WT-D172N, and WT-D172N + 4 μM quinidine conditions. (c) and (d) The maximal spatial gradient of APD₉₀ in WT-D172N and D172N conditions, respectively.

Discussion

Summary of the major findings

The proband with the *KCNJ2* D172N mutation had a QT_c interval of 315 ms, where her 35-year-old father had a QT_c of 320 ms (Priori *et al* 2005). There is clinical evidence to demonstrate the efficacy of quinidine in patients with SQTs (Gaita *et al* 2004, Wolpert *et al* 2005, Kaufman, 2007, Milberg *et al* 2007). Gaita *et al* reported that hydroquinidine prolonged a QT interval, which increased from 263 ± 12 ms to 362 ± 25 ms (calculated QT from 290 ± 13 ms to 405 ± 26 ms). Wolpert *et al* described that quinidine was an effective drug for SQTs with a mutation in *HERG* by restoring normal rate dependence of the QT interval and rendering ventricular tachycardia (VT)/ventricular fibrillation (VF) non-inducible. In the present study, with the use of quinidine, mimicking the effects on SQT3, we found that the QT interval extended from 322 ms to 380, 395, and 397 ms in the presence of 4, 7, and 10 μM quinidine, which is within the normal range of QT interval between 363 and 421 ms.

Our major findings are as follows. (i) Quinidine prolonged APD of the ventricular cells. (ii) Quinidine prolonged ventricular cell APD₉₀ inhomogeneously across the strand, thereby decreased the maximal membrane potential heterogeneity (δV) and decreased transmural

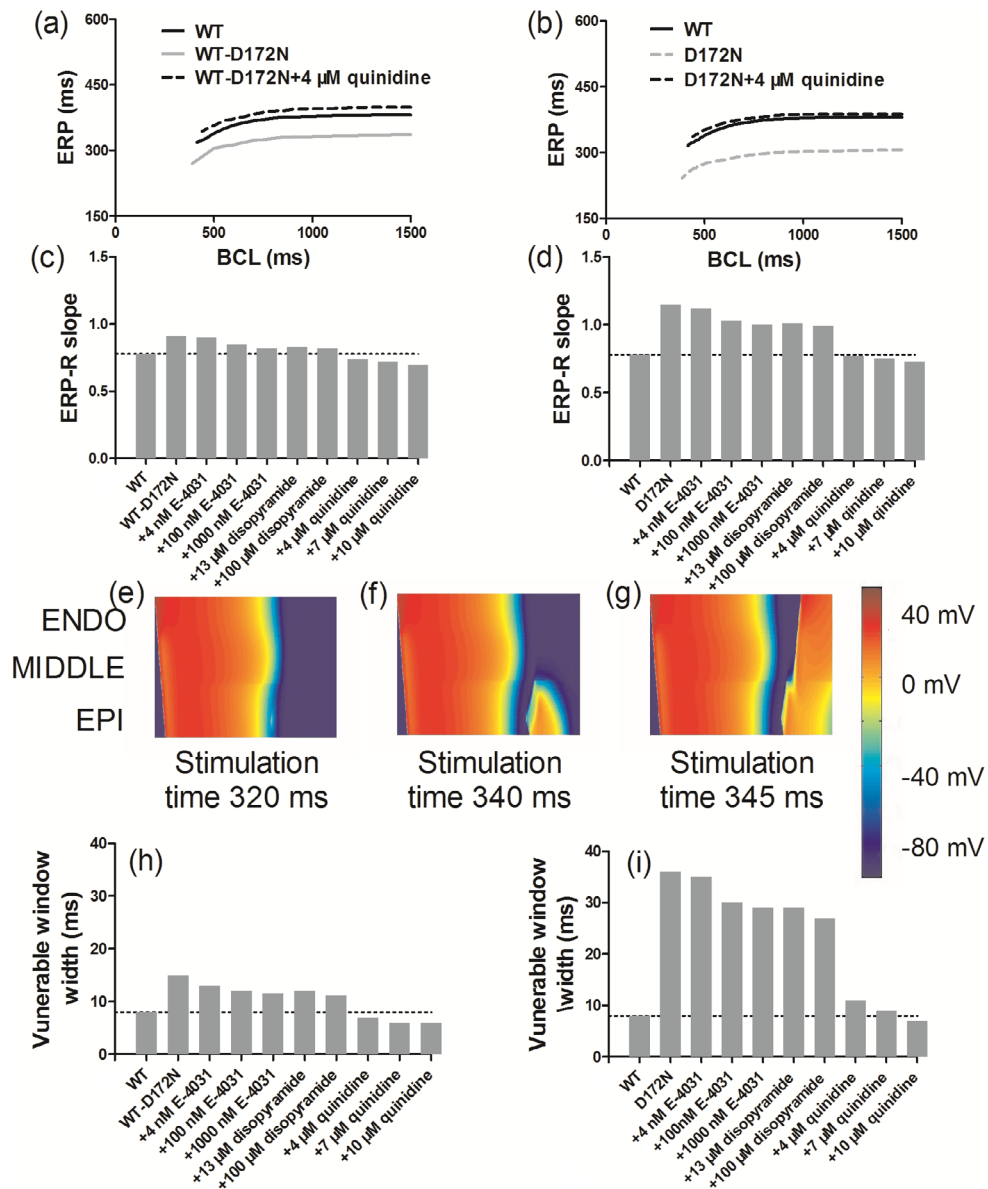


Figure 6. Rate-dependent ERP and vulnerable window in WT, WT-D172N, D172N, and drug-in-action conditions. (a) and (b) Rate-dependent ERP restitution (ERP-R) curves in WT-D172N and D172N conditions, respectively. (c) and (d) Slopes of ERP-R curves in WT-D172N and D172N conditions, respectively. (e) Bidirectional conduction block. (f) Unidirectional conduction block. (g) Bidirectional conduction. (h) and (i) Measured VW width in WT-D172N and D172N conditions, respectively.

dispersion, which combined to contribute the decreased T-wave amplitude. (iii) Quinidine increased ERP and reduced temporal and increased spatial vulnerability to initiate and sustain re-entry, resulting in a reduced susceptibility of ventricular tissue associated with SQT3 to arrhythmogenesis. (iv) Quinidine prevented and terminated re-entrant excitation waves.

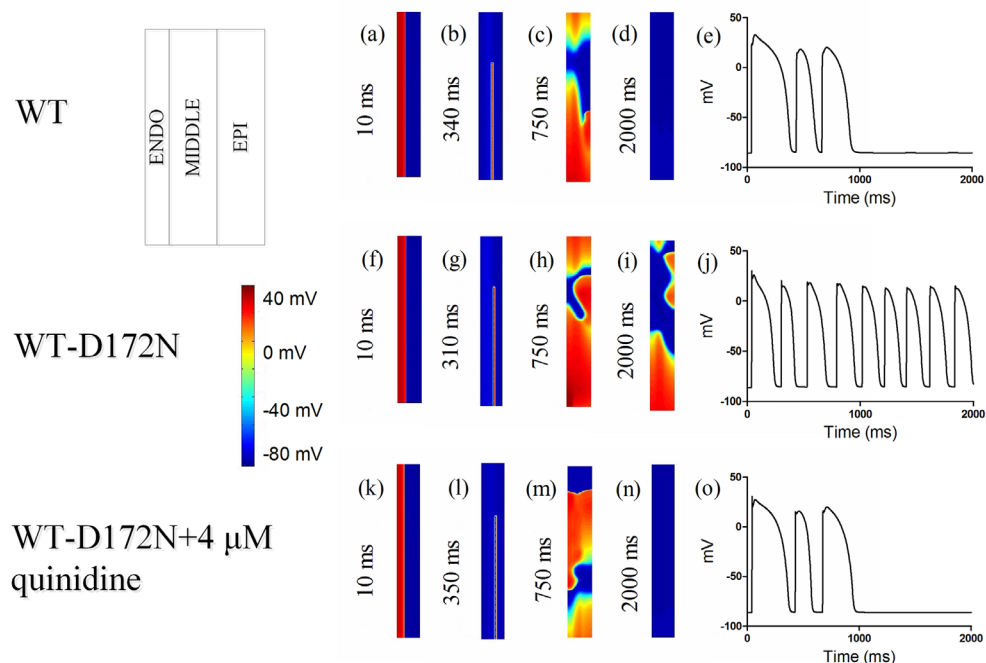


Figure 7. Simulated drug effects in 2D idealized human ventricular tissue, with standard excitation parameters, of size $15\text{ mm} \times 150\text{ mm}$, and of the standard S1-S2 protocol. (a), (f) and (k) A planar wave generated by S1 at the ENDO distal end in the WT, WT-D172N, WT-D172N + $4\ \mu\text{M}$ quinidine conditions, respectively. Snapshot at time = 10 ms. (b), (g) and (l) The S2 was applied to the MIDDLE-EPI junction during the VW of the tissue (WT: 340 ms; WT-D172N: 310 ms; WT-D172N + $4\ \mu\text{M}$ quinidine: 350 ms). (c), (h) and (m) Developed re-entrant excitation waves. Snapshots at time = 750 ms. (d), (i) and (n) Snapshots of the re-entrant excitation waves at time = 2000 ms. Quinidine terminated re-entrant excitation waves in the WT-D172N condition. (e), (j) and (o) Evolution of the AP of a cell in WT, WT-D172N, and WT-D172N + $4\ \mu\text{M}$ quinidine conditions, respectively.

(v) Quinidine exhibited significantly better therapeutic effects on SQT3 than disopyramide and E-4031.

Antiarrhythmic mechanisms of quinidine on SQT3

Our data constitute new evidence that the anti-arrhythmic effects of quinidine on SQT3 associated with Kir2.1 D172N mutation involve both decrease tissue susceptibility to the initiation of re-entry and prevention and termination of re-entry (terminating VF). An increase in ERP generated by actions of quinidine prolonged the wavelength of ventricular excitation waves and less likelihood for re-entrant excitation wave to be formed in a limited ventricular tissue mass. We found that, once formed, re-entry was unstable in the presence of quinidine.

Tissue susceptibility to the genesis of re-entry can be indexed by its temporal and spatial vulnerability. In our simulations, quinidine prolonged ventricular repolarization time due to the prolongation of APD and ERP, and subsequently resulted in a decreased temporal vulnerability (the width of VW). However, prolongation of ERP markedly increased the critical size of the re-entrant substrate, leading to an increased spatial vulnerability to re-entry. This provides a means for decreased ventricular tissue susceptibility to re-entry with the use of quinidine.

Limitations

The ten Tusscher and Panfilov (2006) model was used here to simulate cellular electrical AP of human ventricular myocytes; potential limitations of this model have been discussed elsewhere (ten Tusscher and Panfilov 2006, Zhang *et al* 2008, Adeniran *et al* 2011, 2012). This study aimed to predict the effects of drugs on SQT3 by using purely cellular electrophysiology, and as such did not consider the effects of electrical remodelling or fibrosis. Evidence of electrical remodelling in SQT3 is currently lacking; nevertheless, this may play important roles in re-entrant arrhythmias in SQT3. On the other hand, our model did not consider cardiac mechanical contraction, which has previously been suggested to be affected in SQT3 patients (Schimpf *et al* 2008, Adeniran *et al* 2013, Frea *et al* 2015), and may affect the pharmacological effects of drugs on SQT3.

Another limitation is that the action of drugs at the ion channel level did not incorporate voltage-, state-, frequency-dependent block effects. Regarding the experimental conditions, many factors, including oxygen, the concentration of ions, temperature, and pH (Cardona *et al* 2010, Mirams *et al* 2012), which influence the binding of drugs to ion channels would be required and modelled. Nevertheless, whilst it is useful to make potential limitations of the present study explicit, there are not anticipated to change the fundamental conclusions drawn in our study.

Conclusion

Alterations in I_{K1} have previously been implicated in genesis and maintenance of VF associated with SQT3. Significantly, previous studies demonstrated the efficacy of quinidine in patients with SQT3. Our data indicate that quinidine not only helps to terminate re-entry but also decreases the susceptibility of human ventricular tissue to the genesis of re-entry. Our study identifies distinct factors at cell and tissue levels that underlie these antiarrhythmic changes. In conclusion, the findings of this simulation study add to the growing weight of evidence that quinidine may be a potential therapeutic agent for SQT3.

Acknowledgments

The authors thank Dr Ismail Adeniran for useful discussions and thank the editors and the anonymous reviewers for their constructive comments. Financial support was provided by the China Scholarship Council (CSC) (to CL) and the National Natural Science Foundation of China (NSFC) under Grants No. 61571165 and No. 61572152 (to KW and HZ).

Author contributions

KW and HZ: Conceived and designed the experiments. CL: Performed the experiments. LC, KW, and HZ: Analyzed the data. CL: Wrote the manuscript. KW and HZ: Reviewed and edited the manuscript. All authors approved the work for publication.

Conflict of interests

The authors declare that there are no competing interests.

ORCID iDs

Cunjin Luo  <https://orcid.org/0000-0003-3946-1093>

References

- Adeniran I, El Harchi A, Hancox J C and Zhang H 2012 Proarrhythmia in KCNJ2-linked short QT syndrome: insights from modelling *Cardiovascular Res.* **94** 66–76
- Adeniran I, Hancox J C and Zhang H 2013 In silico investigation of the short QT syndrome, using human ventricle models incorporating electromechanical coupling *Front. Physiol.* **4** 166
- Adeniran I, McPate M J, Witchel H J, Hancox J C and Zhang H 2011 Increased vulnerability of human ventricle to re-entrant excitation in hERG-linked variant 1 short QT syndrome *PLoS Comput. Biol.* **7** e1002313
- Antzelevitch C et al 2007 Loss-of-function mutations in the cardiac calcium channel underlie a new clinical entity characterized by ST-segment elevation, short QT intervals, and sudden cardiac death *Circulation* **115** 442–9
- Bellocq C, van Ginneken A C, Bezzina C R, Alders M, Escande D, Mannens M M, Baro I and Wilde A A 2004 Mutation in the KCNQ1 gene leading to the short QT-interval syndrome *Circulation* **109** 2394–7
- Brennan T, Fink M and Rodriguez B 2009 Multiscale modelling of drug-induced effects on cardiac electrophysiological activity *Eur. J. Pharm. Sci.* **36** 62–77
- Brugada R et al 2004 Sudden death associated with short-QT syndrome linked to mutations in HERG *Circulation* **109** 30–5
- Cardona K, Trenor B, Molto G, Martinez M, Ferrero J M Jr, Starmer F and Saiz J 2010 Exploring the role of pH in modulating the effects of lidocaine in virtual ischemic tissue *Am. J. Physiol. Heart Circ. Physiol.* **299** H1615–24
- Crumb W J Jr, Vicente J, Johannesen L and Strauss D G 2016 An evaluation of 30 clinical drugs against the comprehensive *in vitro* proarrhythmia assay (CiPA) proposed ion channel panel *J. Pharmacol. Toxicol. Methods* **81** 251–62
- Frea S, Giustetto C, Capriolo M, Scrocco C, Fornengo C, Benedetto S, Bianchi F, Pidello S, Morello M and Gaita F 2015 New echocardiographic insights in short QT syndrome: More than a channelopathy? *Heart Rhythm.* **12** 2096–105
- Gaita F, Giustetto C, Bianchi F, Schimpf R, Haissaguerre M, Calo L, Brugada R, Antzelevitch C, Borggrefe M and Wolpert C 2004 Short QT syndrome: pharmacological treatment *J. Am. College Cardiol.* **43** 1494–9
- Gaita F, Giustetto C, Bianchi F, Wolpert C, Schimpf R, Riccardi R, Grossi S, Richiardi E and Borggrefe M 2003 Short QT Syndrome: a familial cause of sudden death *Circulation* **108** 965–70
- Gima K and Rudy Y 2002 Ionic current basis of electrocardiographic waveforms: a model study *Circ. Res.* **90** 889–96
- Gussak I, Brugada P, Brugada J, Wright R S, Kopecky S L, Chaitman B R and Bjerregaard P 2000 Idiopathic short QT interval: a new clinical syndrome? *Cardiology* **94** 99–102
- Izumi D, Chinushi M, Iijima K, Ahara S, Komura S, Furushima H, Hosaka Y, Sanada A, Yagihara N and Aizawa Y 2010 Effects of bepridil versus E-4031 on transmural ventricular repolarization and inducibility of ventricular tachyarrhythmias in the dog *Pacing Clin. Electrophysiol.* **33** 950–9
- Kaufman E S 2007 Quinidine in short QT syndrome: an old drug for a new disease *J. Cardiovascular Electrophysiol.* **18** 665–6
- Kramer J, Obejero-Paz C A, Myatt G, Kuryshev Y A, Bruening-Wright A, Verducci J S and Brown A M 2013 MICE models: superior to the HERG model in predicting Torsade de pointes *Sci. Rep.* **3** 2100
- McPate M J, Duncan R S, Hancox J C and Witchel H J 2008 Pharmacology of the short QT syndrome N588K-hERG K⁺ channel mutation: differential impact on selected class I and class III antiarrhythmic drugs *Br. J. Pharmacol.* **155** 957–66
- McPate M J, Duncan R S, Witchel H J and Hancox J C 2006 Disopyramide is an effective inhibitor of mutant HERG K⁺ channels involved in variant 1 short QT syndrome *J. Mol. Cell Cardiol.* **41** 563–6
- Milberg P, Tegelkamp R, Osada N, Schimpf R, Wolpert C, Breithardt G, Borggrefe M and Eckardt L 2007 Reduction of dispersion of repolarization and prolongation of postrepolarization refractoriness

- explain the antiarrhythmic effects of quinidine in a model of short QT syndrome *J. Cardiovascular Electrophysiol.* **18** 658–64
- Mirams G R, Davies M R, Cui Y, Kohl P and Noble D 2012 Application of cardiac electrophysiology simulations to pro-arrhythmic safety testing *Br. J. Pharmacol.* **167** 932–45
- O'Hara T, Virag L, Varro A and Rudy Y 2011 Simulation of the undiseased human cardiac ventricular action potential: model formulation and experimental validation *PLoS Comput. Biol.* **7** e1002061
- Priori S G *et al* 2005 A novel form of short QT syndrome (SQT3) is caused by a mutation in the KCNJ2 gene *Circ. Res.* **96** 800–7
- Sanchez-Chapula J A 1999 Mechanism of transient outward K(+) channel block by disopyramide *J. Pharmacol. Exp. Ther.* **290** 515–23
- Schimpf R, Antzelevitch C, Haghi D, Giustetto C, Pizzuti A, Gaita F, Veltmann C, Wolpert C and Borggrefe M 2008 Electromechanical coupling in patients with the short QT syndrome: further insights into the mechanoelectrical hypothesis of the U wave *Heart Rhythm.* **5** 241–5
- Schimpf R, Wolpert C, Bianchi F, Giustetto C, Gaita F, Bauersfeld U and Borggrefe M 2003 Congenital short QT syndrome and implantable cardioverter defibrillator treatment: inherent risk for inappropriate shock delivery *J. Cardiovascular Electrophysiol.* **14** 1273–7
- Schimpf R, Wolpert C, Gaita F, Giustetto C and Borggrefe M 2005 Short QT syndrome *Cardiovascular Res.* **67** 357–66
- Taggart P, Sutton P M, Opthof T, Coronel R, Trimlett R, Pugsley W and Kallis P 2000 Inhomogeneous transmural conduction during early ischaemia in patients with coronary artery disease *J. Mol. Cell Cardiol.* **32** 621–30
- Templin C *et al* 2011 Identification of a novel loss-of-function calcium channel gene mutation in short QT syndrome (SQT5) *Eur. Heart J.* **32** 1077–88
- ten Tusscher K H and Panfilov A V 2006 Alternans and spiral breakup in a human ventricular tissue model *Am. J. Physiol. Heart Circ. Physiol.* **291** H1088–100
- Weingart R 1977 The actions of ouabain on intercellular coupling and conduction velocity in mammalian ventricular muscle *J. Physiol.* **264** 341–65
- Wettwer E, Scholtysik G, Schaad A, Himmel H and Ravens U 1991 Effects of the new class III antiarrhythmic drug E-4031 on myocardial contractility and electrophysiological parameters *J. Cardiovascular Pharmacol.* **17** 480–7
- Wolpert C *et al* 2005 Further insights into the effect of quinidine in short QT syndrome caused by a mutation in HERG *J. Cardiovascular Electrophysiol.* **16** 54–8
- Wu L, Guo D, Li H, Hackett J, Yan G X, Jiao Z, Antzelevitch C, Shryock J C and Belardinelli L 2008 Role of late sodium current in modulating the proarrhythmic and antiarrhythmic effects of quinidine *Heart Rhythm.* **5** 1726–34
- Xie F, Qu Z, Garfinkel A and Weiss J N 2002 Electrical refractory period restitution and spiral wave reentry in simulated cardiac tissue *Am. J. Physiol. Heart Circ. Physiol.* **283** H448–60
- Yasuda C, Yasuda S, Yamashita H, Okada J, Hisada T and Sugiura S 2015 The human ether-a-go-go-related gene (hERG) current inhibition selectively prolongs action potential of midmyocardial cells to augment transmural dispersion *J. Physiol. Pharmacol.* **66** 599–607
- Zhang H, Kharche S, Holden A V and Hancox J C 2008 Repolarisation and vulnerability to re-entry in the human heart with short QT syndrome arising from KCNQ1 mutation—a simulation study *Prog. Biophys. Mol. Biol.* **96** 112–31
- Zhang Y H and Hancox J C 2002 Mode-dependent inhibition by quinidine of Na⁺-Ca²⁺ exchanger current from guinea-pig isolated ventricular myocytes *Clin. Exp. Pharmacol. Physiol.* **29** 777–81